Research Square

Preprints are preliminary reports that have not undergone peer review.
They should not be considered conclusive, used to inform clinical practice,
or referenced by the media as validated information.

# Fertilized plant egg cell establishes a rapid block to additional sperm fusion for facilitating double fertilization

**Meng-Xiang Sun**

mxsun@whu.edu.cn

Wuhan University https://orcid.org/0000-0002-6959-8405

**Ce Shi**

Wuhan University https://orcid.org/0000-0002-8920-8750

**Xuecheng Zhang**

Wuhan University https://orcid.org/0000-0001-8667-4740

**Pan Luo**

Wuhan University

**Zifu Zhao**

Wuhan University

**Tao Wan**

Core Botanical Gardens/Wuhan Botanical Garden

**Wei Wang**

Wuhan University

**Siling Li**

Wuhan University

**Hong Chen**

Wuhan University

**Xiaorong Huang**

Xiamen University https://orcid.org/0000-0003-1924-143X

**Tianhe Cheng**

Wuhan University

**Han Xu**

Core Botanical Gardens/Wuhan Botanical Garden

**Jiapeng Han**

Core Botanical Gardens/Wuhan Botanical Garden

**Zhiming Liu**

Core Botanical Gardens/Wuhan Botanical Garden

**Peng Zhao**

Wuhan University https://orcid.org/0000-0003-1904-8955

**Xiongbo Peng**

Wuhan University https://orcid.org/0000-0002-9436-5072

**Ming Yang**

Oklahoma State University https://orcid.org/0000-0002-7499-3338

**Thomas Dresselhaus**

University of Regensburg https://orcid.org/0000-0001-6442-4302

---

**Article**

**Keywords:**

**Posted Date:** November 20th, 2026

**DOI:** https://doi.org/10.21203/rs.3.rs-11427882/v1

**License:** This work is licensed under a Creative Commons Attribution 4.0 International License.
Read Full License

**Additional Declarations:** There is **NO** Competing Interest.

---

# Fertilized plant egg cell establishes a rapid block to additional sperm fusion for facilitating double fertilization

**Authors:**

Ce Shi[1,2,6], Xuecheng Zhang[1,2,6], Pan Luo[1], Zifu Zhao[1], Tao Wan[3], Wei Wang[1], Siling Li[1], Hong Chen[1], Xiaorong Huang[1], Tianhe Cheng[1], Han Xu[3], Jiapeng Han[3], Zhiming Liu[3], Peng Zhao[1], Xiongbo Peng[1], Ming Yang[4], Thomas Dresselhaus[5], Meng-Xiang Sun[1,2]*

**Affiliations:**

[1]State Key Laboratory of Hybrid Rice, College of Life Sciences, Wuhan University, Wuhan, 430072, China

[2]College of Life Sciences, Guizhou Normal University, Guiyang, 550025, China

[3]Core Botanical Gardens/Wuhan Botanical Garden, Chinese Academy of Sciences, Wuhan, 430074, China

[4]Department of Plant Biology, Ecology, and Evolution, Oklahoma State University, 301 Physical Sciences, Stillwater, OK, 74078-1010, USA

[5]Cell Biology and Plant Biochemistry, University of Regensburg, Regensburg, 93053, Germany

[6]These authors contributed equally

*Correspondence: mxsun@whu.edu.cn

**Abstract:**

In angiosperms, the mechanism by which the egg cell fuses with only one sperm and prevents fusion with additional sperm has long been a mystery. Here, we report that the two aspartic endopeptidases ECS1/2 secreted from egg cells following egg-sperm fusion cleave the ectodomain of the conserved fusogen HAP2/GCS1 on the sperm cell surface. This cleavage disables further HAP2/GCS1-mediated egg-sperm fusions while preserving central cell-sperm fusion, thus effectively preventing egg cell polyspermy and facilitating double fertilization, as well as maintaining the genetic stability of offspring. We further show that this ingenious molecular machinery evolved in three steps originating from common ancestors of land plants. This co-evolved ECS-HAP2/GCS1 module represents an essential strategy for ensuring successful double fertilization.

**Main Text:**

During sexual reproduction, genetic stability requires that each egg fuse with a single sperm, as polyspermy is actively prevented[1]. In many animals, this is achieved through egg-secreted proteases that modify the zona pellucida and block secondary sperm-egg fusion[2–4]. Unlike animals and early land plants, such as mosses and ferns, flowering plants (angiosperms) have evolved a unique reproductive strategy for preventing polyspermy. Each pollen tube in angiosperms delivers two nonmotile sperm cells to the embryo sac containing two female gametes (egg cell and central cell). Following pollen tube rupture, one sperm fuses with the egg and the other fuses with the central cell, a process known as double fertilization[5].

Since double fertilization was first described over a century ago[6,7], a central question has been how flowering plants ensure that each female gamete is fertilized only once for maintaining successful double fertilization. Although fertilization of the egg and central cell are often considered nearly simultaneous[8,9], live-cell imaging in *Arabidopsis* has revealed an average interval of approximately 2.5 min between the two fertilization events[9]. During this brief window, both sperm cells remain functionally equivalent and lack a predetermined fertilization fate[10,11]. Successful double fertilization therefore requires mechanisms that rapidly establish a polyspermy block immediately after the first gamete fusion.

Evidence for such a polyspermy block is provided when excess sperm are present. When fertilization failure triggers fertilization-recovery mechanisms that attract multiple pollen tubes into the ovule, the egg cell still undergoes monospermic fertilization[12–14]. Likewise, in *tetraspore* (*tes*) mutant pollen, where the egg is simultaneously confronted with multiple sperm, the egg cell remains monospermic while the central cells can accept additional sperm[15,16]. These findings support the hypothesis that when the egg cell is first fertilized, the fertilization may rapidly trigger a mechanism that prevents additional sperm-egg fusion during the period in which the central cell is not yet fertilized[9].

Although known observations are consistent with the hypothesis, the mechanism underlying the rapid and egg-specific block to polyspermy remains unclear[15–20]. It was reported that fertilization could induce transient $Ca^{2+}$ rise in eggs in both plants and animals, and sperm fusion with isolated rice or maize egg protoplasts *in vitro* also induced cell wall deposition, which may contribute to the polyspermy block[18,21–27]. However, these slower mechanisms do not yet explain how the egg cell establishes a rapid polyspermy block at the gamete level immediately after successful fertilization. Thus, the molecular basis of the egg-specific block to additional sperm-egg fusion remains poorly understood.

**ECS1/2 establish a fast egg cell-specific polyspermy block**

To address this long-standing question and to elucidate the underlying molecular mechanism, we searched for *Arabidopsis* egg cell-specific genes and focused on two genes, *Egg Cell Specific 1* and *2* (*ECS1/2*), which encode aspartic endopeptidases[28]. Our previous studies revealed that ECS1 and ECS2 are secreted from the egg cell upon successful fertilization to degrade the pollen tube attractant LURE1, thereby preventing the enticement of additional pollen tubes (polytubey) and indirectly contributing to polyspermy prevention[28]. To determine whether *ECS1/2* are also involved in a direct and rapid egg-regulated block, we introduced an egg cell plasma membrane marker *pDD45::GFP-LTI6b*[29] into Columbia-0 (Col-0, wild type) and *ecs1/2* plants and the marker lines were pollinated with *HTR10-mRFP* Col-0 pollen. In Col-0 × Col-0 crosses, polyspermy was not observed in either the egg or central cell (0/745, 0/682, and 0/657; Fig. 1a). In contrast, in *ecs1/2* × Col-0 crosses, the second sperm fusion with the fertilized egg cell was repeatedly observed. Z-stack confocal imaging and 3D reconstruction revealed both completed polyspermic events, in which two sperm nuclei were present within the egg cell (Fig. 1b,c, Extended Data Fig. 1a,c–e, and Supplementary Video 1–4), and ongoing polyspermic events, in which the second

sperm was fusing with the egg cell (Extended Data Fig. 2f–h and Supplementary Video 5–7). These polyspermy events were detected in 7 of 2031 *ecs1/2* ovules (3/756, 2/619, and 2/656), compared with 0 of 2084 Col-0 ovules (two-sided Fisher's exact test, $P = 0.0072$). Although rare, the repeated detection of the polyspermic events indicates that loss of *ECS1/2* compromises the egg-cell-autonomous barrier against additional sperm incorporation during fertilization under normal two-sperm conditions.

Building on this observation, we next examined whether the ECS1/2-dependent barrier can prevent egg cell polyspermy when multiple sperm cells are available. We generated a *tes* mutant in the *HTR10-mRFP* background using CRISPR-Cas9 (Extended Data Fig. 2a). In *tes* mutant, 15.8% of pollen grains contained more than two sperm cells: 14.5% had four and 1.3% had six sperm cells (Fig. 1d and Extended Data Fig. 2b). Next, we pollinated *pDD45::GFP-LTI6b* marker lines in Col-0 and *ecs1/2* backgrounds with *tes* pollen. To specifically evaluate the behavior of *ecs1/2* eggs under multiple-sperm conditions, only the ovules receiving more than two sperm cells were further analyzed. In Col-0 × *tes* crosses, 84% of ovules completed double fertilization with the extra sperm remaining unfertilized; in the remaining 16%, additional sperm entered the central cell. Notably, no egg cell polyspermy was detected in Col-0 × *tes* crosses (Fig. 1e,f). In contrast, *ecs1/2* × *tes* ovules showed similar rates of double fertilization (82.5%), but extra sperm nuclei were detected both in egg cells (14%) and central cells (3.5%), as confirmed by Z-stack confocal imaging and 3D reconstruction (Extended Data Fig. 1b and Supplementary Video 11). Complementation with catalytically inactive ECS1/2 variants ($ECS1^{D103N,D324N}$ and $ECS2^{D103N,D326N}$) failed to rescue the polyspermy phenotype, demonstrating that the proteolytic activity of ECS1/2 is required for this block (Fig. 1f). Together, these results reveal that ECS1/2 function to directly prevent egg cell polyspermy under normal two-sperm condition and especially under multiple-sperm conditions.

To genetically validate whether *ecs1/2* egg cells undergo polyspermy, we analyzed the ploidy of progeny from *ecs1/2* × *tes* crosses. Seeds were initially grouped by size (Groups I–III), as embryo ploidy correlates with seed size (Fig. 1g)[15]. Ploidy was determined by flow cytometry and chromosome spreads of male meiocytes at anaphase I (Fig. 1h,i). Most seedlings from normal-sized seeds (Group I) were diploid (2n), with 98.3% in Col-0 × *tes* and 99% in *ecs1/2* × *tes* crosses (Fig. 1j). In larger seeds (Group II), polyploid seedlings (>2n) were detected in 5.4% of Col-0 × *tes* and 15.1% of *ecs1/2* × *tes* progeny (Fig. 1j and Extended Data Fig. 2c). Since *tes* pollen produce sperm of varying ploidy (1n–4n), triploid (3n) or tetraploid (4n) offspring could arise from a single

fertilization event and thus do not unambiguously indicate polyspermy[15]. By contrast, pentaploid (5n) seedlings can only result from the fusion of a haploid egg with multiple sperm, because pentaploid embryos derived from a haploid egg and a tetraploid sperm are nonviable (Extended Data Fig. 2d)[15]. Therefore, the surviving 5n seedlings necessarily reflect multiple-sperm fertilization of the egg. Notably, *ecs1/2* × *tes* crosses yielded 3.8% of pentaploid offspring in Group II, a phenomenon never observed in Col-0 × *tes* crosses (Fig. 1j). These results further support the essential role of *ECS1/2* in establishing a robust barrier against additional sperm-egg fusion during double fertilization.

**ECS1/2 directly cleave the ectodomain of the fusogen HAP2**

To further investigate how ECS1/2 block egg polyspermy, we tested whether ECS1/2 can bind and cleave egg-sperm fusogens. HAPLESS 2 [HAP2, also called GENERATIVE CELL SPECIFIC 1 (GCS1), hereafter referred to HAP2] is considered as an ancient conserved cell fusogen and the only confirmed fusogen in flowering plants to date[30–40]. We therefore examined potential interactions between ECS1/2 and HAP2. Using membrane-based yeast two-hybrid (MbY2H) assays, both ECS1/2 specifically interacted with HAP2, and further analysis showed binding to the HAP2 ectodomain (ECD) rather than its intracellular domain (ICD) (Fig. 2a). The HAP2-ECD consists of three structured domains (DI–DIII) followed by a stem region that links the ECD to the transmembrane domain[30]. Furthermore, pull-down assays confirmed that ECS1/2 specifically bind HAP2-(DIII–stem) region (Fig. 2b), whereas DI–DIII fragments lacking the stem did not interact (Extended Data Fig. 3a,b). Together, these findings identify HAP2 as a direct interactor and putative proteolytic substrate of ECS1/2.

To determine whether HAP2 is a direct substrate of ECS1/2, we performed *in vitro* proteolysis assays. Incubation of the HAP2-(DIII–stem) with either a low amount of ECS1 or ECS2 generated distinct cleavage products (Fig. 2c) and increase of enzyme-to-substrate ratios further enhanced cleavage efficiency within 2 min (Fig. 2d). Furthermore, using PROSPER (PROtease Specificity Prediction servER)[41], we identified four putative cleavage sites (s1–s4) of aspartic protease in the HAP2-ECD and synthesized corresponding fluorogenic peptides (P1–P4) (Fig. 2e and Extended Data Fig. 3c,d). Kinetic analysis showed that both ECS1 and ECS2 efficiently cleave these peptides, with P1 and P4 exhibiting the highest cleavage efficiency (Fig. 2f). Molecular docking predicted preferential interactions of the two ECS active sites with the s1 and s4 cleavage sites of HAP2, consistent with the *in vitro* cleavage results (Extended Data Fig. 3e–l). Next, we chose P4

as a representative site to study site-specific cleavage of HAP2 by ECS1/2, since cleavage at this position efficiently removes nearly the entire HAP2-ECD, which is critical for sperm-egg fusion[42]. Mutations of Leucine (L), Valine (V), and Phenylalanine (F) decreased the cleavage efficiency of ECS1; mutations of L, V, Aspartic acid (D), and F decreased the cleavage efficiency of ECS2 (Fig. 2g). To assess HAP2 processing in planta, we co-expressed a truncated HAP2 lacking the intracellular domain with wild-type or inactive ECS1/2 in *Nicotiana benthamiana* leaves. Compared with the inactive variants, wild-type ECS1/2 markedly reduced HAP2 accumulation, suggesting protease activity-dependent HAP2 processing *in vivo* (Fig. 2h). Together, these results establish HAP2 as a direct proteolytic substrate of ECS1/2.

Due to the low frequency of polyspermy phenotypes observed in *ecs1/2*, we wondered whether gene redundancy might be responsible for the weak phenotype. Interestingly, we found that when *ECS1/2* were mutated, a compensatory protease EMAP1 (*ECS1/2* mutation-promoted aspartic protease 1), which is barely expressed in the wild-type egg cells, could be triggered and expressed (Extended Data Fig. 4a–d). We further confirm that EMAP1 could also interact with HAP2 and cleave its ectodomain, thus functioning as functional compensation for the loss of *ECS1/2* (Extended Data Fig. 4e–g). This explains why the low frequency of egg polyspermy was detected in *ecs1/2* mutants. In fact, it is reasonable that multilayered backup system may have evolved to ensure successful double fertilization, which is essential for both alternation of generations and population reproduction.

**Sperm-surface HAP2 ectodomain preferentially promotes sperm-egg fusion**

To assess the effects of deletions in HAP2-ECD on gamete fusion, we generated transgenic lines that were supplemented with homozygous HAP2 variants driven by the native *HAP2* promoter and introduced them into the HTR10-mRFP/*hap2*/+ background. Based on the higher cleavage efficiency of ECS1/2 for site s1 and s4 of HAP2 (Fig. 2f), and the location of site s2 and s3 in beta folds inside HAP2 (Extended Data Fig. 3d), we chose HAP2-s1 (cleavage site s1) and HAP2-s4 to test their effect on sperm fusion ability with egg and central cells, respectively (Fig. 3a and Extended Data Fig. 5a). In addition, HAP2-N (lacking ICD) and HAP2-C (lacking ECD) were employed to evaluate the contributions of distinct HAP2 domains to gamete fusion (Extended Data Fig. 5a). HAP2-s1 and HAP2-N exhibited similar localization patterns to full-length HAP2-GFP, while HAP2-s4 and HAP2-C showed abnormal localization patterns (Fig. 3b and Extended Data Fig. 5b). To test whether HAP2-s1 remains activatable, we performed an *in vitro* sperm cell

activation assay using EC1 peptide[43,44]. HAP2-s1 could be efficiently recruited to the sperm plasma membrane like unmodified HAP2 (Fig. 3c). In contrast, HAP2-s4 failed to translocate to the membrane, indicating a loss of responsiveness to EC1 and rendering it non-functional (Extended Data Fig. 5c). We next evaluated *in vivo* sperm-egg fusion competency of these HAP2 variants. Full-length HAP2-GFP completely rescued this sperm-egg fusion defect in *hap2*/+ mutants, confirming full functionality (Fig. 3d,e). In contrast, HAP2-N showed 26.5% (n = 375) and 24.3% (n = 367) of unfused gametes, demonstrating that HAP2-ICD is required for sperm function. Similarly, HAP2-s1 could only partially complement the *hap2*/+ phenotype, with rescue rates of 26.9% and 27.4% (Fig. 3e). Nevertheless, HAP2-s1 preferentially impaired sperm-egg fusion while permitting central cell fusion, with rates of 0.35% and 0.20% for egg cell single fertilization versus 9.23% and 10.72% for central cell single fertilization (Fig. 3f,g). This ~1:32 preference for egg over central cell fusion suggests that the intact HAP2-ECD on the sperm plasma membrane is preferentially required for sperm-egg fusion compared with sperm-central cell fusion.

To further confirmed this differential requirement for sperm-surface HAP2-ECD during fusion with egg and central cell, we mimicked ECS-mediated HAP2-ECD removal while minimizing confounding effects of HAP2 truncation on fusion competence prior to sperm activation. Using a previously established *DMP8/9* (*DOMAIN OF UNKNOWN FUNCTION 679 MEMBRANE PROTEIN 8/9*)-dependent trafficking system, overexpression of *NTL11ΔC* (*NAC TRANSCRIPTION FACTOR-LIKE 11 lacking the C-terminal transmembrane domain*) in the *dmp8/9* background produced single sperm-like cells (SLCs)[10,44]. These cells expressed full-length HAP2 normally but fail to localize it to sperm plasma membrane, SLCs lacking plasma membrane-localized HAP2-ECD (Fig. 3h)[10,44,45]. Following pollination, we analyzed embryo and endosperm development by co-expressing the egg-cell/zygote nuclear marker *pDD45::H2B-GFP* and the central-cell/endosperm marker *pDD22::H2B-GFP* (Fig. 3i)[10]. In contrast to Col-0 SLCs, which preferentially fused with egg cells (112 egg versus 1 central cell fusion event), *dmp8/9* SLCs exhibited a strong bias toward central cell fusion (1 egg versus 104 central cell fusion events; two-sided Fisher's exact test, $P < 0.0001$) (Fig. 3j). Altogether, these results suggest that loss of sperm-surface HAP2-ECD mainly compromises sperm-egg fusion while largely preserving sperm-central cell fusion, providing a mechanistic explanation for how ECS-mediated removal of sperm-surface HAP2-ECD could establish an egg-specific polyspermy block.

## Stepwise emergence of the ECS-HAP2 regulatory module

To further understand the evolution of the ECS-HAP2 module and its role in the establishment of a block to polyspermy, we analyzed (i) the origin of ECS endopeptidases, (ii) their evolutionary history, and (iii) the possible interaction and co-evolution of ECS and HAP2 across green plants (Viridiplantae). ECS1/2 belong to the aspartic protease (AP) family, whose members participate in diverse developmental and physiological processes[46]. Analysis of 23 representative green plant (including chlorophytes, charophytes, bryophytes, ferns, gymnosperms, and angiosperms) genomes identified 1457 AP proteins, which could be classified into three major clades (AP-A, AP-B, and AP-C) (Fig. 4a; Extended Data Table 1,2). *Arabidopsis* ECS1/2 belong to the AP-C clade. Notably, AP-C homologs were absent from chlorophytes and most charophytes, and only two copies of AP-C genes were identified in *Mesotaenium endlicherianum* (Zygnemophyceae), a group of streptophyte algae representing a sister lineage of land plants[47]. By contrast, a considerable amplification of AP-C members was observed in the Embryophyta (Extended Data Table 2).

To trace the evolutionary history of AtECS1/2, we constructed an additional maximum-likelihood tree composed of all homologous genes identified in our AP dataset with *Arabidopsis* AP-A subfamily genes *At1G69100* and *At4G22050* as random controls (Extended Data Fig. 6). Genes from chlorophytes, charophytes, ferns, gymnosperms, 'basal' angiosperms, and monocots formed an outgroup relative to eudicot genes, while eudicot genes resided on three distinct branches. Each branch contained genes from grape, poplar and Brassicales, which was likely caused by the γ-whole-genome triplication event (γ-WGT), a keystone genetic event that occurred in the common ancestor of all core eudicots (Extended Data Fig. 6)[48,49]. Combining syntenic analysis with the synonymous substitutions per synonymous site (*Ks*) distribution of all paralogous pairs (including *AtECS1/2*) among *A. thaliana–A. thaliana*, *A. thaliana–Boechera stricta*, and *A. thaliana–Capsella rubella* revealed an obvious *Ks* peak before *Ks* peaks of the Brassicaceae speciation events (Fig. 4b and Extended Data Fig. 7). This suggests that the α-whole-genome duplication event (α-WGD) occurring in the common ancestor of the Brassicaceae species[50] led to the divergence of AtECS1/2 from their common ancestral archetypal gene. This finding might also explain functional redundancy and moderate substrate divergence of AtECS1/2 reported above (Fig. 2f), which is typical for 'recent' WGD-derived duplicates[51].

The early origin of the ECS homologous lineage (AP-C-clade) in Zygnemophyceae encouraged

us to further clarify its subsequential diversification across Embryophyta. A total of six different types of protein structures were predicted from 196 records of homologous ECSs in green plants (Fig. 4c and Extended Data Table 3). Notably, type IV, which also includes AtECS1/2, is commenced in bryophytes and gradually overrepresented in other Embryophyta lineages (Fig. 4c,d). All land plants share a relative conserved ECS motif composition, while corresponding proteins from aquatic Charophytes like *Chara braunii* and *M. endlicherianum* contain an incomplete motif (Extended Data Fig. 8). We next studied the expression profile of ECS in different plant clades and found three ECS homologs [Pp3C13_14230 (type IV), Pp3c3_17600 (type IV), and Pp3c19_10740 (type V)] in the bryophyte *Physcomitrium patens*. The corresponding genes showed a very general expression pattern in different cells and tissues including the eggs[52]. By contrast, egg-specific expression of *ECSs* was observed in the 'basal' angiosperm *Amborella trichopoda* and the monocot *Oryza sativa*[53,54], which implies that functional divergence/specification might have occurred in angiosperms (Fig. 4e and Extended Data Table 4,5). Transcriptomic data from gymnosperm and fern egg cells would help to elucidate whether egg cell-specific expression is indeed restricted to angiosperms. With regard to interaction between ECS and HAP2, we next characterized the divergence history of HAP2 in the Viridiplantae. In general, there exist only one or two *HAP2* or *HAP2*-like genes across green plant lineages in each species as previously noted also for other eukaryotes (Extended Data Fig. 9)[30]. We could separate two types of 3D-structures of HAP2 (type I and II) in examined species (Fig. 4f,g and Extended Data Fig. 10). Similar ECDs between *Arabidopsis* and *C. braunii* (Charophytes) indicate the early origin of HAP2 in Viridiplantae (Fig. 4g). Notably, we found that a relatively uniform motif composition emerged in flowering plants, which is different from a more variable pattern that occurred in seed-free plants (Fig. 4g, Extended Data Fig. 11, and Extended Data Table 4). Moreover, the potential cleavage sites of APs in HAP2 are concentrated in DI–DIII in seed-free plants, while cleavage sites of APs in angiosperm HAP2 have been shifted to the DI–DII and the stem. This suggests putative functional divergence (Fig. 4c and Supplementary Text). In particular, the novel cleavage site in the stem that is particular important for ECS-HAP2 interaction appears to be specifically important in dicotyledonous species where it is highly conserved.

To further validate the evolutionary hypothesis (Fig. 4h), we employed the *AtECS2* promoter to drive egg cell-specific expression of *ECS* orthologs from diverse species (including *P. patens*, *A. trichopoda*, *O. sativa*, *Populus trichocarpa*, *Cleome violacea*, and *Capsella rubella*) in *ecs1/2* mutant (Fig. 5a and Extended Data Fig. 12). Phenotypic analysis revealed functional divergence

among ECS proteins. Notably, dicot ECS variants (CvECS, CrECS, and PtECS) successfully rescued the fertility defects of *ecs1/2*, including seed set, polytubey, and egg polyspermy (Fig. 5b–f). The restoration of seed set and polytubey is consistent with previous reports linking *ECS1/2* to seed development and polytubey blocking[28,55,56]. Importantly, dicot *ECS* orthologs also restored the egg polyspermy block, whereas ECS proteins from non-dicot lineages failed to restore (Fig. 5f). These results suggest that the function of ECS in preventing egg polyspermy is conserved among dicot species, but is not broadly conserved across green plants. This pattern coincides with the emergence and conservation of a dicot-enriched AP cleavage site within the HAP2 stem region (Fig. 4g), consistent with the possibility that ECS and HAP2 underwent coordinated functional specialization during angiosperm evolution.

**Discussion:**

In flowering plants, strict prevention of egg polyspermy is essential for successful double fertilization and genetic stability of offspring, as polyspermy causes aberrant nuclear divisions and early embryonic lethality[19,20]. Despite extensive study in animals since Just's early observations in 1919[57], the molecular basis of polyspermy block in plants remained largely unknown. We previously reported that ECS1/2 form a cortical network in eggs and are specifically secreted upon sperm-egg fusion, reminiscent of secretory networks described in animal eggs[28]. Here, we provide genetic, biochemical, and cell biological evidence consistent with a model in which ECS1/2 cleave the fusogen HAP2-ECD right after fertilization, thereby contributing to the prevention of additional sperm-egg fusion. Consistently, *ecs1/2* mutants allow multiple sperm to enter the egg cell. Thus, ECS-HAP2 machinery defines a post-fertilization mechanism that rapidly reinforces egg monospermy in angiosperms. We also reveal that ECS-HAP2 machinery is only part of the complex network for the egg cell preventing polyspermy. When ECS1/2 were mutated, compensatory proteases EMAP1 could be triggered to express, which also functions to cleave HAP2 ectodomain. Thus, ECS-HAP2 pathway represents a rapid-responding machinery in the network for robust egg monospermy. More components of this network remain to be further identified.

Double fertilization involves both egg-sperm and central cell-sperm fusion. In *hap2* null mutants, the entire absence of full HAP2 function in *hap2* null mutants resulted in failure of both egg and central cell fertilization, confirming HAP2 is required for double fertilization[58]. In this work, the sperm lacking surface-exposed intact HAP2-ECD (in HAP2-s1 or *dmp8/9* SLCs) preferentially fused with the central cell, a phenotype also observed in *gcs1*$^{GAA}$[59]. By contrast, perturbation of the HAP2-ICD biases fertilization toward the egg cell[42]. These observations reveal an intrinsic asymmetry in the requirements for HAP2 function between the two female gametes. However, these domain-specific effects require proper HAP2 expression and localization at the sperm plasma membrane. Therefore, domain-perturbation approaches, rather than a *hap2* null background, allow to examine how ECS-mediated modification of the HAP2 ectodomain differentially affects egg-cell and central-cell fusion. As suggested by evidence described above, ECS cleavage disables HAP2-mediated egg-sperm fusions but does not affect central cell-sperm fusion, revealing a more detailed layer of HAP2 function.

The ECS-HAP2 machinery functions regardless of gamete fusion order reported previously[8]. If the central cell is fertilized first, a block to additional sperm entry established[16]. In this case, the egg cell remains unfertilized and therefore does not yet require a mechanism to prevent the sperm-egg fusion. Conversely, if the egg cell is fertilized first, ECS1/2 secretion may rapidly cleave HAP2-ECD on the remaining sperm, thereby reducing sperm-egg fusion competence to prevent egg cell polyspermy while preserving sperm-central cell fusion. The protective role of the ECS-HAP2 machinery becomes particularly evident when multiple sperm cells are delivered into the embryo sac. In this case, as evidenced in this work, the egg cell remained monospermy, but central cell polyspermy was easily observed. This could also explain the previously-reported different ability in preventing polyspermy between egg cell and central cell[15,16]. Evolutionarily, sperm-egg fusion is ancestral in land plants, whereas sperm-central cell fusion emerged later in angiosperms.[60] The ECS-HAP2 module likely evolved to contribute to egg polyspermy prevention, while central cell fusion remains less restricted. Theoretically, acceptance of multiple sperm by the central cell may also help reduce polyspermy risk in the egg cell, indicating complementary strategies that reinforce fertilization fidelity.

In short, our finding suggests that ECS-mediated regulation of HAP2 introduces an additional regulatory layer to the fusogen function[61], revealing a direct and rapid post-fusion inactivation mechanism that ensures egg monospermy. Three key insights emerge. (i) Post-fusion inactivation of fusogens is crucial for fertilization fidelity. Although degradation or internalization of fusexins such as *Chlamydomonas Cr*HAP2[62] and *Caenorhabditis elegans Ce*EFF-1[63] has been reported, our work provides the direct biochemical evidence in plants. (ii) Double fertilization requires strict spatiotemporal precision: two sperm are delivered simultaneously adjacent to the egg, and ECS1/2 secretion immediately after egg fertilization is proposed to quickly restrict additional sperm-egg fusion, complementing slower $Ca^{2+}$-dependent processes, such as zygote wall formation[18,22]. (iii) Sperm-egg fusion depends strongly on HAP2-ECD integrity, as proteolytic disruption impair fusion, paralleling irreversible transitions reported for viral class II fusexins and EFF-1[64,65]. This suggests that HAP2-ECD may function as a regulatory module controlling fusion activity whose conformational stability is essential for membrane merger, and its proteolytic sensitivity reflects an evolutionary conservation of fusion regulation across kingdoms.

Finally, we propose a three-step evolutionary trajectory for the ECS-HAP2 polyspermy block (Fig. 4h). (i) An early *ECS* emergence supported by type IV *ECS* expression in the eggs of *P. patens*[53]

and its absence in Charophytes/Chlorophytes, with polyspermy instead prevented by ECS-independent, glycosylation-dependent HAP2 degradation in *C. reinhardtii*[62]. (ii) Specialized HAP2 motifs, shifted cleavage sites, and expansion of type II HAP2 in angiosperms; the increased cleavage sites in HAP2-DII may have contributed to the loss of the ancestral fusion loop[30,35]. (iii) Optimization in dicot angiosperms, where AtECS1/2 preferentially target the HAP2 stem region, potentially enables more rapid HAP2 inactivation. This trajectory highlights how incremental molecular innovations in the ECS-HAP2 module contributes to a fast and robust egg polyspermy block in land plants. Future work will explore how diverse proteolytic strategies regulate HAP2 across green plants and other eukaryotes.

## Methods

### Plant materials and growth conditions

T-DNA insertion *esc1/2* double mutant lines used in this study are as previously described[28]. T-DNA insertion line *gcs1* (SALK_135496) was obtained from the Arabidopsis Biological Resource Center (ABRC). *Arabidopsis thaliana* Columbia-0 (Col-0) was used as wild-type. *tes* mutants were generated using the clustered regularly interspaced short palindromic repeats (CRISPR)-associated protein 9 (Cas9) system[67]. The CRISPR target of *TES* was selected as previously described[68], and vectors were transferred into *HTR10-mRFP*/Col-0. The genomic region surrounding the CRISPR target site of *TES* was amplified by PCR, and the segment subjected to Sanger sequencing to identify mutants. Primer sequences are listed in Extended Data Table 6. *Arabidopsis* plants were grown in soil in a greenhouse under long-day conditions (16 h light/8 h dark) at 22°C.

### Ploidy analyses

Ploidy analysis was performed by employing two different methods as previously described: flow cytometry and chromosome spreading[55,69]. For flow cytometry, two leaves were harvested and chopped using a razor blade in a petri dish with 500 μL of nuclei extraction buffer (Partec CyStain UV Precise-Kit). Then, 1 mL of staining reagent (Partec CyStain UV Precise-Kit) was added, and specimens were incubated at room temperature for 1 min. After filtration, the samples were detected by using a Beckmann CytoFlex ploidy analyzer. For meiosis chromosome spreading, flower buds fixed in Carnoy's solution were washed twice with 10 mM citrate buffer (pH 4.5) and digested with 0.3% cellulose and 0.3% pectolyase in citrate buffer for 1 h at room temperature. After being washed twice with the same buffer and after adding DAPI solution (10 μg/mL), digested flower buds were squashed with a cover slip to release epollen mother cells (PMCs) and samples were observed using a Leica SP8 CLSM.

### Confocal microscopy and image analysis

Samples were imaged using a Leica TCS SP8 confocal laser scanning microscope. GFP was excited at 488 nm, with emission collected between 498–550 nm. RFP was excited at 552 nm, and its emission collected between 600–650 nm. 3D image reconstruction and rendering were performed using Aivia AI software (Leica Microsystems) enabling precise spatial analysis of fluorescence signal distribution. The relative localization of HTR10-mRFP–labeled sperm nuclei was analyzed with respect to the GFP-LTI6b–labeled egg cell membrane using Z-stack confocal imaging and 3D reconstruction. Secondary sperm entry events were classified based on the spatial

position of the second sperm nucleus relative to the egg cell boundary, including sperm nuclei positioned outside, at the periphery of, or within the egg cell. Diffuse or reduced HTR10-mRFP fluorescence of the first sperm nucleus was considered consistent with sperm nuclear decondensation following sperm-egg fusion.

**DUAL membrane yeast two-hybrid assays**

Membrane-based split-ubiquitin yeast two-hybrid assays were performed according to the DUAL membrane starter kit manual (Dualsystems Biotech). In brief, yeast strain NMY51 was co-transformed with a bait and prey vector and protein-protein interactions were scored based on growth on SD-X-gal (β-galactosidase) medium lacking leucine, tryptophane, adenine and histidine (-L-W-H-A) for 5 days. *ECS1* and *ECS2* were cloned into the prey vector pPR3-N. HAP2 and deletions were cloned in pBT3-C. All primers used to generate the different deletions are listed in Extended Data Table 6.

**Pull-down assays**

To express maltose binding protein (MBP)-ECS1 and MBP-ECS2 fusion proteins in *Escherichia coli*, *ECS1* and *ECS2* lacking the signal peptide sequence were cloned into the vector pMAL-c2X and purified as previously described[28]. HAP2-(DI-DIII)-His fusion protein was expressed in human embryonic kidney 293 (HEK293F) cells via the pSecTag vector and purified by fractionation with ammonium sulfate by DIA-AN. The HAP2-(DIII-stem) domain was cloned into the vector pET32a and the His-HAP2-(DIII-stem)-His fusion protein thereafter expressed in *E. coli* BL21. Purification was performed as previously described using Ni-NTA His Bind Resin (Merck) according to the manufacturer's instructions.

For pull-down assays, MBP-ECS1, MBP-ECS2, and MBP were mixed with HAP2-(DI-DIII)-His and His-HAP2-(DIII-stem)-His, respectively, incubated with 40 µL of equilibrated MBP-Trap agarose beads (ChromoTek) resuspended in 400 µL of buffer containing 10 mM Tris/HCl pH 7.5, 150 mM NaCl, 0.5 mM EDTA for 1 h at 4°C. Then the mixture was spun down at 2500× *g* for 5 min. After removing the supernatant, the resin was extensively rinsed with 500 µL of the same buffer to remove unbound proteins and washed five times. Finally, resuspend beads in 80 µL 2× SDS-sample buffer was boiled for 5 min at 95°C to dissociate immunocomplexes from beads. Beads were sedimented by centrifugation at 2500× *g* for 2 min at 4°C and supernatants separated

in SDS-PAGE, blotted and Western blots incubated with anti-MBP (1:5000 dilution; NEB) and anti-His (1:2000 dilution; Abcam), respectively.

**Egg cell isolation and semiquantitative RT-PCR**

Egg cell isolation, RNA extraction, and reverse transcription from *ecs1/2* and Col-0 plants were performed as previously described[70]. Semiquantitative RT-PCR was performed to examine the expression of *ECS1*, *ECS2*, and *EMAP1* genes in isolated egg cells.

**AP cleavage assays**

The coding region of *ECS* and *EMAP1* lacking the putative signal peptide sequences was amplified and inserted into the pPIC9K vector (Invitrogen). Plasmid DNA was linearized and electroporated into *Pichia pastoris* (strain GS115) cells according to the manufacturer's instructions. Yeast was grown in buffered glycerol complex (BMGY) medium and transferred into buffered methanol complex (BMMY) medium with 0.5% methanol for expression induction when optical density at $OD_{600} = 2.5$ was reached. After 3 days of induction, the culture supernatant containing the secreted ECS fusion protein was collected. Subsequently, the remaining culture medium was replaced with acetic acid buffer (50 mM NaAc, 5% glycerol, pH 6.0) for cleavage assays.

The Flag-HAP2-(DIII-stem) domain was cloned into the vector pET32a and the Flag-HAP2-(DIII-stem) fusion protein thereafter expressed in *E. coli* BL21. Purification was performed as previously described using Ni-NTA His Bind Resin according to the manufacturer's instructions. The Flag-HAP2-(DIII-stem) and ECS1/2 proteins were added to NaAC buffer (pH 6.0) and incubated at 25°C for cleavage assays. Proteins were detected by immunoblotting using an anti-Flag antibody (1:2000 dilution; ABclonal).

To investigate the proteolytic activity of recombinant ECS1 and ECS2 against HAP2, fluorogenic peptide substrates and related mutations were designed, synthesized (GenScript) and used for proteolytic activity determination. Peptides were labelled with MCA and DNP at both ends[28,71]. Fluorescence levels were monitored using a Cytation3 cell imaging reader (BioTek) with excitation and emission filters of 328 and 393 nm, respectively.

**Molecular docking analysis**

Molecular docking analysis was performed using AutoDock to evaluate the potential interaction between ECS1 catalytic sites (As1 and As2) and the four predicted HAP2 cleavage sites (s1–s4).

The docking scores were calculated to compare the predicted interaction preferences of different ECS1-HAP2 combinations. The lowest-energy docking models were selected for visualization.

**Transient co-expression of ECS and HAP2 in *Nicotiana benthamiana***

To assess ECS-mediated cleavage of HAP2 in planta, the CDSs of ECS1, ECS2, and their catalytically inactive variants ($ECS1^{D103N,D324N}$ and $ECS2^{D103N,D326N}$), excluding the N-terminal signal peptide sequences, were amplified from previously generated constructs[28] and fused in frame with GFP at the C terminus. An HA epitope tag was inserted at amino acid 493 of HAP2(1–595), upstream of the predicted ECS cleavage site 4 in the stem region, generating the HAP2-HA construct. All expression cassettes were cloned into a plant expression vector under the control of the *CaMV 35S* promoter and introduced into *Agrobacterium tumefaciens* strain GV3101. Agrobacterium cultures carrying the indicated constructs were infiltrated into fully expanded leaves of 4-week-old *N. benthamiana* plants. Leaf tissues were harvested 24 h after infiltration. For each biological replicate, three infiltrated leaf regions from independent leaves were pooled to minimize variation in transient expression. Samples were immediately frozen in liquid nitrogen and ground to a fine powder. Total proteins were extracted in extraction buffer (25 mM Tris-HCl, pH 7.4, 100 mM NaCl, 1% Triton X-100, 5% glycerol [v/v], 1× protease inhibitor mixture [Roche]) for 1 h at 4°C with gentle rotation. Protein extracts were subjected to SDS-PAGE and immunoblot analysis using anti-GFP, anti-HA, and anti-Actin antibodies (ABclonal). Primary antibodies were used at a dilution of 1:2000 and HRP-conjugated secondary antibodies at 1:5000 (ABclonal). Band intensities were quantified using ImageJ. HAP2-HA signals were first normalized to the corresponding Actin signals. The normalized HAP2-HA level in samples co-expressing catalytically inactive ECS variants was set to 1, and relative HAP2-HA accumulation in samples co-expressing wild-type ECS proteins was calculated accordingly. Three independent biological replicates were analyzed.

**Sperm cell activation assay**

A modified semi-*in vivo* pollen germination assay was performed to assess sperm cell activation. Mature, unpollinated pistils were manually pollinated with transgenic pollen grains expressing HAP2-s1 and HAP2-s4 variants, respectively. The pistils were then cut at the junction between the style and ovary. The upper portion of each pistil was positioned vertically on a 35-mm petri dish containing solidified pollen germination medium (PGM)[44]. Following a 2-h incubation under humid conditions, pistils were transferred into droplets of liquid PGM and further incubated for

6–7 h. Two high-performance liquid chromatography (HPLC)-purified synthetic peptides corresponding to the EC1.1 signature motifs[37], S1 (CSGELILFFLNGETYIGPG) and S2 (CWPTMIGVLGFTAQEGDMLQGY), were synthesized by GenScript. Lyophilized peptides were dissolved in DMSO, briefly sonicated, and diluted with 100 mM Tris-HCl buffer (pH 7.7) to reach 20% (v/v) DMSO. This solution was further diluted to 1:20 with liquid PGM to achieve a final peptide concentration of 120 μM for each peptide in 2% DMSO. A peptide-free control containing only 2% DMSO in liquid PGM was used as a negative control. To release sperm cell pairs, pollen tubes growing out from the style were gently severed using a sterile surgical blade. Samples were then carefully covered with a coverslip and incubated for 10 min in a moist chamber prior to microscopic observation.

**Evolutionary history of the AP gene family**

Aspartic protease domains (PF00026, PF03489, PF05184, PF14541 and PF14534)[72,73] were used to search AP protein sequences against a local database containing genome sequences of 23 green plant species from chlorophytes to angiosperms by HMMER search. Protein sequences obtained were used as queries to conduct reverse Blastp searches against the same local database. All retrieved sequences were scanned in the PFAM database. Only proteins with aspartic protease domains were retained. After aligned with MAFFT (L-INS-i) and trimmed with TrimAL (-gt 0.6), AP proteins with a length longer that 100 aa were used to produce a maximum likelihood (ML) tree in FastTree (JTT+CAT+Gamma20). Reciprocal all-against-all comparisons for *A. thaliana–A. thaliana*, *A. thaliana–Boechera stricta*, and *A. thaliana–Capsella rubella* were performed using the Blastp program. Syntenic blocks were computed in MCScanX with default parameter (-k 50 -s 5 -m 25). Ks values of syntenic gene pairs were estimated in ParaAT using MAFFT and KaKs_Calculator.

**Motif identification and prediction of 3D-protein structures**

To investigate protein structure types of *ECS* and *HAP2* in green plants, we used the software of SWISS-MODEL (https://swissmodel.expasy.org/interactive) as a prediction tool. For each type of proteins, the number was counted, and the protein type was named (I, II, III, IV, V and VI) according to the time of their occurrence from green alga to flowering plants on the phylogenetic tree. To further identify and analyze motifs of these proteins' amino acid sequences, MEME (https://meme-suite.org/meme/tools/meme) was used as method for motif discovery, and MEGA

(https://www.megasoftware.net/) version 6.0 to construct a phylogenetic tree. The neighbor-joining algorithm with 1000 bootstrap replicates was used in this analysis.

**Statistical analysis**

The dot and box-and-whisker plots were prepared by Student's *t*-test, two-side Fisher's exact test, and Tukey-Kramer multiple comparison test for statistical analysis by using the GraphPad Prism v.9.0.0. software.

**References:**


1. Deneke, V. E. & Pauli, A. The fertilization enigma: how sperm and egg fuse. *Annu. Rev. Cell Dev. Biol.* **37**, 391–414 (2021).
2. Katzberg, A. A. & Hendrickx, A. G. Gonadotropin-induced anomalies of the zona pellucida of the baboon ovum. *Science* **151**, 1225–1226 (1966).
3. Gahlay, G. et al. Gamete recognition in mice depends on the cleavage status of an egg's zona pellucida protein. *Science* **329**, 216–219 (2010).
4. Nishio, S. et al. ZP2 cleavage blocks polyspermy by modulating the architecture of the egg coat. *Cell* **187**, 1440–1459 (2024).
5. Berger, F., Hamamura, Y., Ingouff, M. & Higashiyama, T. Double fertilization—caught in the act. *Trends Plant Sci.* **13**, 437 (2008).
6. Nawashin, S. G. Resultate einer Revision der Befruchtungsvorgänge bei *Lilium martagon* und *Fritillaria tenella* L. *Bull. Acad. Imp. Sci. St Pétersbourg* **9**, 377 (1898).
7. Guignard, M. L. Sur les anthérozoides et la double copulation sexuelle chez les végétaux angiospermes. *Rev. Gén. Bot.* **11**, 129 (1899).
8. Faure, J. E., Rotman, N., Fortuné, P. & Dumas, C. Fertilization in *Arabidopsis thaliana* wild type: developmental stages and time course. *Plant J.* **30**, 481–488 (2002).
9. Hamamura, Y. et al. Live-cell imaging reveals the dynamics of two sperm cells during double fertilization in *Arabidopsis thaliana*. *Curr. Biol.* **21**, 497–502 (2011).
10. Wang, W. et al. EGG CELL 1 contributes to egg-cell-dependent preferential fertilization in Arabidopsis. *Nat. Plants* **10**, 268–282 (2024).
11. Li, L. et al. The egg cell is preferentially fertilized in Arabidopsis double fertilization. *J. Integr. Plant Biol.* **64**, 2039–2046 (2022).
12. Kasahara, R. D. et al. Fertilization recovery after defective sperm cell release in *Arabidopsis*. *Curr. Biol.* **22**, 1084–1089 (2012).
13. Maruyama, D. et al. Independent control by each female gamete prevents the attraction of multiple pollen tubes. *Dev. Cell* **25**, 317–323 (2013).
14. Beale, K. M., Leydon, A. R. & Johnson, M. A. Gamete fusion is required to block multiple pollen tubes from entering an *Arabidopsis* ovule. *Curr. Biol.* **22**, 1090–1094 (2012).
15. Scott, R. J., Armstrong, S. J., Doughty, J. & Spielman, M. Double fertilization in *Arabidopsis thaliana* involves a polyspermy block on the egg but not the central cell. *Mol. Plant* **1**, 611–619 (2008).
16. Nagahara, S., Takeuchi, H. & Higashiyama, T. Polyspermy block in the central cell during double fertilization of *Arabidopsis thaliana*. *Front. Plant Sci.* **11**, 588700 (2021).
17. Faure, J. E., Digonnet, C. & Dumas, C. An *in vitro* system for adhesion and fusion of maize gametes. *Science* **263**, 1598–1600 (1994).
18. Kranz, E., Wiegen, P. & Lörz, H. Early cytological events after induction of cell division in egg cells and zygote development following *in vitro* fertilization with angiosperm gametes. *Plant J.* **8**, 9–23 (1995).

19. Nakel, T. et al. Triparental plants provide direct evidence for polyspermy induced polyploidy. *Nat. Commun.* **8**, 1033 (2017).

20. Grossniklaus, U. Polyspermy produces tri-parental seeds in maize. *Curr. Biol.* **27**, R1300–R1302 (2017).

21. Antoine, A. F. et al. Differential contribution of cytoplasmic $Ca^{2+}$ and $Ca^{2+}$ influx to gamete fusion and egg activation in maize. *Nat. Cell Biol.* **3**, 1120–1123 (2001).

22. Denninger, P. et al. Male-female communication triggers calcium signatures during fertilization in *Arabidopsis*. *Nat. Commun.* **5**, 4645 (2014).

23. Digonnet, C., Aldon, D., Leduc, N., Dumas, C. & Rougier, M. First evidence of a calcium transient in flowering plants at fertilization. *Development* **124**, 2867–2874 (1997).

24. Hamamura, Y. et al. Live imaging of calcium spikes during double fertilization in *Arabidopsis*. *Nat. Commun.* **5**, 1–9 (2014).

25. Uchiumi, T., Uemura, I. & Okamoto, T. Establishment of an *in vitro* fertilization system in rice (*Oryza sativa* L.). *Planta* **226**, 581–589 (2007).

26. Toda, E., Ohnishi, Y. & Okamoto, T. Development of polyspermic rice zygotes produced *in vitro*. *Plant Physiol.* **171**, 206–214 (2016).

27. Bleckmann, A., Alter, S. & Dresselhaus, T. The beginning of a seed: regulatory mechanisms of double fertilization. *Front. Plant Sci.* **5**, 452 (2014).

28. Yu, X. et al. Fertilized egg cells secrete endopeptidases to avoid polytubey. *Nature* **592**, 433–437 (2021).

29. Kurup, S. et al. Marking cell lineages in living tissues. *Plant J.* **42**, 444–453 (2005).

30. Fedry, J. et al. Evolutionary diversification of the HAP2 membrane insertion motifs to drive gamete fusion across eukaryotes. *PLoS Biol.* **16**, e2006357 (2018).

31. Mori, T., Kuroiwa, H., Higashiyama, T. & Kuroiwa, T. GENERATIVE CELL SPECIFIC 1 is essential for angiosperm fertilization. *Nat. Cell Biol.* **8**, 64–71 (2006).

32. Liu, Y. et al. The conserved plant sterility gene HAP2 functions after attachment of fusogenic membranes in *Chlamydomonas* and *Plasmodium* gametes. *Genes Dev.* **22**, 1051–1068 (2008).

33. Hirai, M. et al. Male fertility of malaria parasites is determined by GCS1, a plant-type reproduction factor. *Curr. Biol.* **18**, 607–613 (2008).

34. Cole, E. S. et al. Function of the male-gamete-specific fusion protein HAP2 in a seven-sexed ciliate. *Curr. Biol.* **24**, 2168–2173 (2014).

35. Kawai-Toyooka, H. et al. Sex-specific posttranslational regulation of the gamete fusogen GCS1 in the isogamous volvocine alga *Gonium pectorale*. *Eukaryot. Cell* **13**, 648–656 (2014).

36. Ebchuqin, E. et al. Evidence for participation of GCS1 in fertilization of the starlet sea anemone *Nematostella vectensis*: implication of a common mechanism of sperm-egg fusion in plants and animals. *Biochem. Biophys. Res. Commun.* **451**, 522–528 (2014).

37. Okamoto, M. et al. Two HAP2-GCS1 homologs responsible for gamete interactions in the cellular slime mold with multiple mating types: implication for common mechanisms of

584 sexual reproduction shared by plants and protozoa and for male-female differentiation. *Dev.*
585 *Biol.* **415**, 6–13 (2016).

586 38. Camacho-Nuez, M. et al. Hap2, a novel gene in *Babesia bigemina* is expressed in tick
587 stages, and specific antibodies block zygote formation. *Parasite Vector* **10**, 568 (2017).

588 39. von Besser, K., Frank, A. C., Johnson, M. A. & Preuss, D. *Arabidopsis* HAP2 (GCS1) is a
589 sperm-specific gene required for pollen tube guidance and fertilization. *Development* **133**,
590 4761–4769 (2006).

591 40. Fédry, J. et al. The ancient gamete fusogen HAP2 is a Eukaryotic class II fusion protein.
592 *Cell* **168**, 904–915 (2017).

593 41. Song, J. et al. PROSPER: an integrated feature-based tool for predicting protease substrate
594 cleavage sites. *PLoS ONE* **7**, e50300 (2012).

595 42. Wong, J. L., Leydon, A. R. & Johnson, M. A. HAP2 (GCS1)-dependent gamete fusion
596 requires a positively charged carboxy-terminal domain. *PLoS Genet.* **6**, e1000882 (2010).

597 43. Sprunck, S. et al. Egg cell-secreted EC1 triggers sperm cell activation during double
598 fertilization. *Science* **338**, 1093–1097 (2012).

599 44. Wang, W. et al. DMP8 and 9 regulate HAP2/GCS1 trafficking for the timely acquisition of
600 sperm fusion competence. *Proc. Natl. Acad. Sci. USA* **119**, e2207608119 (2022).

601 45. Cyprys, P., Lindemeier, M. & Sprunck, S. Gamete fusion is facilitated by two sperm cell-
602 expressed DUF679 membrane proteins. *Nat. Plants* **5**, 253–257 (2019).

603 46. Soares, A. et al. An atypical aspartic protease modulates lateral root development in
604 *Arabidopsis thaliana*. *J. Exp. Bot.* **70**, 2157–2171 (2019).

605 47. Cheng, S. et al. Genomes of subaerial Zygnematophyceae provide insights into land plant
606 evolution. *Cell* **179**, 1057–1067 (2019).

607 48. Jaillon, O. et al. The grapevine genome sequence suggests ancestral hexaploidization in
608 major angiosperm phyla. *Nature* **449**, 463–467 (2007).

609 49. Chanderbali, A. S. et al. *Buxus* and *Tetracentron* genomes help resolve eudicot genome
610 history. *Nat. Commun.* **13**, 643 (2022).

611 50. Bowers, J. E., Chapman, B. A., Rong, J. & Paterson, A. H. Unravelling angiosperm genome
612 evolution by phylogenetic analysis of chromosomal duplication events. *Nature* **422**, 433–
613 438 (2003).

614 51. De Smet, R., Sabaghian, E., Li, Z., Saeys, Y. & Van de Peer, Y. Coordinated functional
615 divergence of genes after genome duplication in *Arabidopsis thaliana*. *Plant Cell* **29**, 2786–
616 2800 (2017).

617 52. Sanchez-Vera, V. et al. The *Physcomitrium patens* egg cell expresses several distinct
618 epigenetic components and utilizes homologues of *BONOBO* genes for cell specification.
619 *New Phytol.* **233**, 2614–2628 (2021).

620 53. Flores-Tornero, M. et al. Transcriptomics of manually isolated *Amborella trichopoda* egg
621 apparatus cells. *Plant Reprod.* **32**, 15–27 (2019).

622 54. Xie, L. et al. RiceENCODE: A comprehensive epigenomic database as a rice Encyclopedia
623 of DNA Elements. *Mol. Plant* **14**, 1604–1606 (2021).

55. Zhang, X. et al. A female in vivo haploid-induction system via mutagenesis of egg cell specific peptidases. *Mol. Plant* **16**, 471–480 (2023).

56. Mao, Y. et al. ECS1 and ECS2 suppress polyspermy and the formation of haploid plants by promoting double fertilization. *eLife* **12**, e85832 (2023).

57. Jaffe, L. A. The fast block to polyspermy: New insight into a century-old problem. *J. Gen. Physiol.* **150**, 1233–1234 (2018).

58. Nagahara, S., Takeuchi, H. & Higashiyama, T. Generation of a homozygous fertilization-defective *gcs1* mutant by heat-inducible removal of a rescue gene. *Plant Reprod.* **28**, 33–46 (2015).

59. Mori, T., Hirai, M., Kuroiwa, T. & Miyagishima, S. The functional domain of GCS1-based gamete fusion resides in the amino terminus in plant and parasite species. *PLoS ONE* **5**, e15957 (2010).

60. Li, H. J. & Yang, W. C. Central cell in flowering plants: specification, signaling, and evolution. *Front. Plant Sci.* **11**, 590307 (2020).

61. Brukman, N. G., Li, H. & Podbilewicz, B. Fusexins, HAP2/GCS1 and evolution of gamete fusion. *Front. Cell Dev. Biol.* **9**, 824024 (2022).

62. Liu, Y., Misamore, M. J. & Snell, W. J. Membrane fusion triggers rapid degradation of two gamete-specific, fusion-essential proteins in a membrane block to polygamy in *Chlamydomonas*. *Development* **137**, 1473–1481 (2010).

63. Smurova, K. & Podbilewicz, B. RAB-5- and DYNAMIN-1-mediated endocytosis of EFF-1 fusogen controls cell-cell fusion. *Cell Rep.* **14**, 1517–1527 (2016).

64. Bressanelli, S. et al. Structure of a flavivirus envelope glycoprotein in its low-pH-induced membrane fusion conformation. *EMBO J.* **23**, 728–738 (2004).

65. Pérez-Vargas, J. et al. Structural basis of eukaryotic cell-cell fusion. *Cell* **157**, 407–419 (2014).

66. Hohmann, N. et al. A time-calibrated road map of Brassicaceae species radiation and evolutionary history. *Plant Cell* **27**, 2770–2784 (2015).

67. Xing, H. et al. A CRISPR/Cas9 toolkit for multiplex genome editing in plants. *BMC Plant Biol.* **14**, 327 (2014).

68. Liu, H. et al. CRISPR-P 2.0: an improved CRISPR-Cas9 tool for genome editing in plants. *Mol. Plant* **10**, 530–532 (2017).

69. Shi, C. et al. Reprogramming of microspore fate via BBM-BAR1 for highly efficient in vivo haploid induction. *Cell* **188**, 6109–6120 (2025).

70. Zhao, P. et al. Two-Step Maternal-to-Zygotic Transition with Two-Phase Parental Genome Contributions. *Dev. Cell* **49**, 554–569 (2019).

71. Simões, I., Faro, R., Bur, D. & Faro, C. Characterization of recombinant CDR1, an *Arabidopsis* aspartic proteinase involved in disease resistance. *J. Biol. Chem.* **282**, 31358–31365 (2007).

72. Beers, E. P., Jones, A. M. & Dickerman, A. W. The S8 serine, C1A cysteine and A1 aspartic protease families in *Arabidopsis*. *Phytochemistry* **65**, 43–58 (2004).

664 73. Chen, J., Ouyang, Y., Wang, L., Xie, W. & Zhang, Q. Aspartic proteases gene family in rice:
665 gene structure and expression, predicted protein features and phylogenetic relation. *Gene*
666 **442**, 108–118 (2009).

667 74. Goodstein, D. M. et al. Phytozome: a comparative platform for green plant genomics.
668 *Nucleic Acids Res.* **40**, D1178–D1186 (2012).

669 75. The UniProt Consortium. UniProt: the universal protein knowledgebase in 2021. *Nucleic*
670 *Acids Res.* **49**, D1 (2021).

671 76. Moller, S., Croning, M. D. R. & Apweiler, R. Evaluation of methods for the prediction of
672 membrane spanning regions. *Bioinformatics* **17**, 646–653 (2001).

673 77. Waterhouse, A. et al. SWISS-MODEL: homology modelling of protein structures and
674 complexes. *Nucleic Acids Res.* **46**, W296–W303 (2018).

675 78. Bienert, S. et al. The SWISS-MODEL Repository—new features and functionality. *Nucleic*
676 *Acids Res.* **45**, D313–D319 (2017).

677 79. Guex, N., Peitsch, M. C. & Schwede, T. Automated comparative protein structure modeling
678 with SWISS-MODEL and Swiss-PdbViewer: A historical perspective. *Electrophoresis* **30**,
679 S162–S173 (2009).

680 80. Studer, G. et al. QMEANDisCo—distance constraints applied on model quality estimation.
681 *Bioinformatics* **36**, 1765–1771 (2020).

682 81. Bertoni, M., Kiefer, F., Biasini, M., Bordoli, L. & Schwede, T. Modeling protein quaternary
683 structure of homo- and hetero-oligomers beyond binary interactions by homology. *Sci. Rep.*
684 **7**, 1–15 (2017).

685

**Acknowledgments:**

We are grateful to Frederic Berger for generously providing the HTR10-mRFP marker line and to Qijun Chen for kindly sharing the pKSE401 and pCBC-DT1T2 vectors. We thank Zhenghui Lu for providing the *Pichia pastoris* strain GS115. We thank Hailong Yan for providing the *Chlamydomonas reinhardtii* (CC125) image and Haiying Yi and Yixuan Yin (Leica Microsystems Trading, Ltd., Shanghai, China) for expert assistance with confocal microscopy analysis and 3D image reconstruction. We also thank Qin Lu, Xinlian Liu, and Zhe Zhang (Wuhan University) for their support with microscopy imaging, Zhuang Yao for assistance with egg cell isolation, and Li Shu (Westlake University) for assistance with protein structure analysis.

**Funding:**

This work was supported by the National Natural Science Foundation of China (32130031, 32600489, 32400278, and U24A20349), the Funding for Discipline Development of Guizhou Province [XKBF(2025)030], the Guizhou Provincial Major Scientific and Technological Program [(2025)042], the China Postdoctoral Science Foundation (2023T160494), and the German Research Foundation via research unit FOR 5098 (ICIPS; DR 334/16-1).

**Author contributions:**

M.-X.S., C.S., and X.Z. designed the research plans. C.S., X.Z., L.P., Z.Z., S.L., H.C., W.W., X.H., T.C., P.Z., M.Y., and X.P. performed the phenotype and genetics analyses. C.S., Z.Z., and S.L. performed the biochemical studies. T.W., C.S., H.X., J.H., and Z.L. performed the evolution analyses. T.D. and M.-X.S. contributed to the data analysis and finalized the manuscript. All authors contributed to data collection, presentation and manuscript writing.

**Competing interests:**

The authors declare no competing interests.

**Data and materials availability:**

All data are available in the main text and the supplementary materials.

**Extended data and supplementary information:**

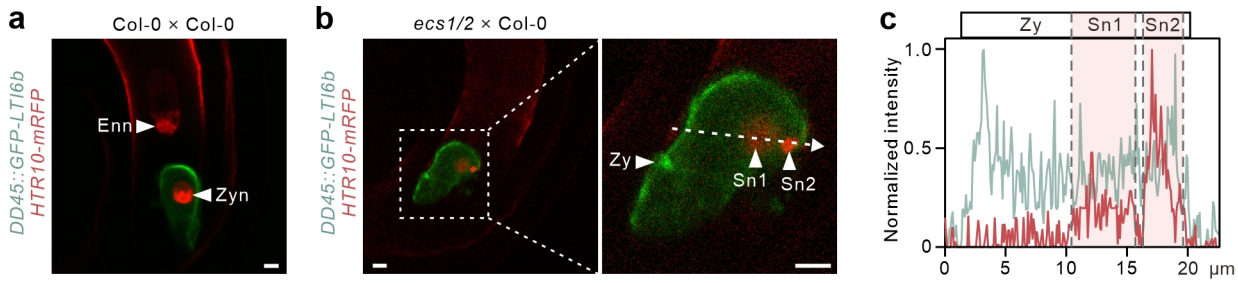
Extended data Figures 1 to 12

Extended data Tables 1 to 6

Supplementary Videos 1 to 11

Supplementary Text

## Figures and Figure legends:




**f**

| Cross (female × male) | Double fertilization | Polyspermy of Cc | Polyspermy of Ec |
|---|---|---|---|
| Col-0 × *tes* | 42 (84%) | 8 (16%) | 0 (0%) |
| *ecs1/2* × *tes* | 118 (82.5%) | 5 (3.5%) | 20 (14.0%) |
| *ecs1/2 ECS1*$^{cat-}$ × *tes* | 105 (83.3%) | 6 (4.8%) | 15 (11.9%) |
| *ecs1/2 ECS2*$^{cat-}$ × *tes* | 92 (83.6%) | 4 (3.6%) | 14 (12.7%) |

**j**

| Cross (female × male) | Group I | | | | Group II | | | |
|---|---|---|---|---|---|---|---|---|
| | 2n | 3n | 4n | 5n | 2n | 3n | 4n | 5n |
| Col-0 × *tes* | 116 | 2 | 0 | 0 | 35 | 1 | 1 | 0 |
| *ecs1/2* × *tes* | 118 | 2 | 0 | 0 | 45 | 4 | 2 | 2* |

**Fig. 1 ECS activity is required to prevent egg polyspermy.**

**a**, Both sperm cells fuse with egg and central cell nuclei in Col-0 (wild-type) ovules. Sperm nuclei are labeled with *HTR10-mRFP*; egg plasm membrane with *pDD45::GFP-LTI6b*. **b**, Both sperm cells fuse with the egg cell in *ecs1/2* mutant. **c**, Fluorescence intensity profiles along the line in (**b**) confirm both sperm nuclei (red) inside the egg cell or now zygote (green). **d**, *HTR10-mRFP*-labeled sperm nuclei in Col-0 and *tes* pollen. **e**, Fertilization pattern with supernumerary sperm from *tes* pollen. (i) Two sperm typically complete double fertilization while extra sperm remain outside (white arrowheads); (ii) one sperm fuses with the egg cell and extra sperm fuse with the central cell (yellow arrowheads); (iii) *ecs1/2* eggs can be fertilized by multiple sperm (asterisks). **f**, Statistics of fertilization patterns with supernumerary sperm. Only ovules receiving extra sperm

were analyzed. ECS1$^{cat-}$ and ECS2$^{cat-}$ are catalytically inactive variants. **g**, Seed size categories after *tes* pollination: normal, enlarged, or shriveled/aborted. **h**, *ecs1/2* × *tes* crosses produced diploid (2n) and pentaploid (5n) progeny. **i**, Chromosome spreads of male meiocytes at anaphase I in 2n and 5n plants. **j**, Seedling ploidy of Col-0 × *tes* and *ecs1/2* × *tes* offspring; asterisk highlights ploidy that could only result from egg polyspermy. Cc, central cell; Ec, egg cell; Enn, endosperm nuclei; Sc, sperm cell; Sn, sperm nuclei; Zyn, zygote nuclei. Scale bars, 5 μm (**a**, **b**, **d**, **e**, and **i**), 50 μm (**g**).

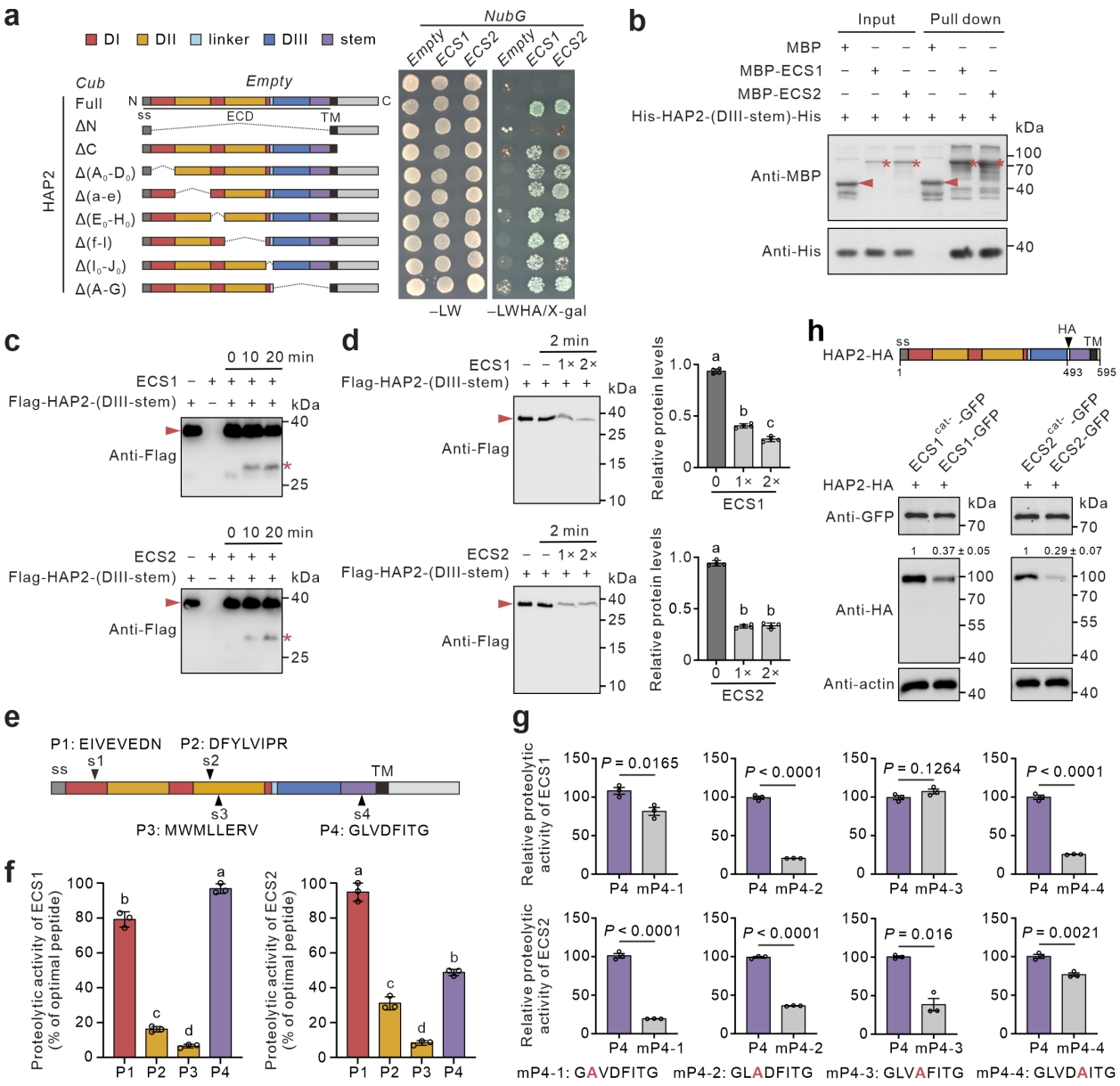



**Fig. 2 ECS1/2 target HAP2 for proteolytic cleavage.**

**a**, ECS1/2 interact with HAP2 ectodomain (ECD) at multiple sites in a membrane-based yeast two-hybrid assay. **b**, ECS1/2 interact with the HAP2-(DIII–stem) in pull-down assays. His-HAP2-(DIII–stem)-His (35.2 kDa) or MBP-ECS1/2 was visualized by immunoblotting using an anti-His or anti-MBP antibody, respectively. Asterisks, MBP-ECS1 (88.2 kDa) and MBP-ECS2 (88.8 kDa) fusion proteins; arrowheads, MBP (50.8 kDa). **c**, Flag-HAP2-(DIII–stem) (37.6 kDa, arrowheads) incubated with ECS1/2 at the indicated time points was detected by immunoblotting using an anti-Flag antibody. Asterisks, the fragments of Flag-HAP2-(DIII-stem) cleaved by ECS1/2. **d**, Increasing the ratio of ECS/Flag-HAP2-(DIII-stem) results in depletion of Flag-HAP2-(DIII-stem)

protein levels (arrowheads) within 2 min. **e**, Position of predicted cleavage sites 1–4 (s1–s4) and related peptides 1–4 (P1–P4) in HAP2. **f**, Proteolytic activity of recombinant ECS1/2 toward fluorogenic peptides P1–P4 derived from predicted HAP2 cleavage sites. **g**, Proteolytic activity of ECS1/2 toward P4 peptides carrying single alanine substitutions. **h**, Immunoblot analysis of the truncated HAP2-HA construct shown above in *Nicotiana benthamiana* co-expressing catalytically inactive or wild-type ECS isoforms. The detected HAP2-HA protein migrated at ~100 kDa, substantially above its predicted molecular mass. The data are shown as the mean ± SD. Different letters indicate significant differences ($P < 0.05$, Tukey-Kramer test) in (**d** and **f**). Statistical significance was assessed by Student's *t*-test in (**g**). ss, signal peptide sequence; TM, transmembrane domain.

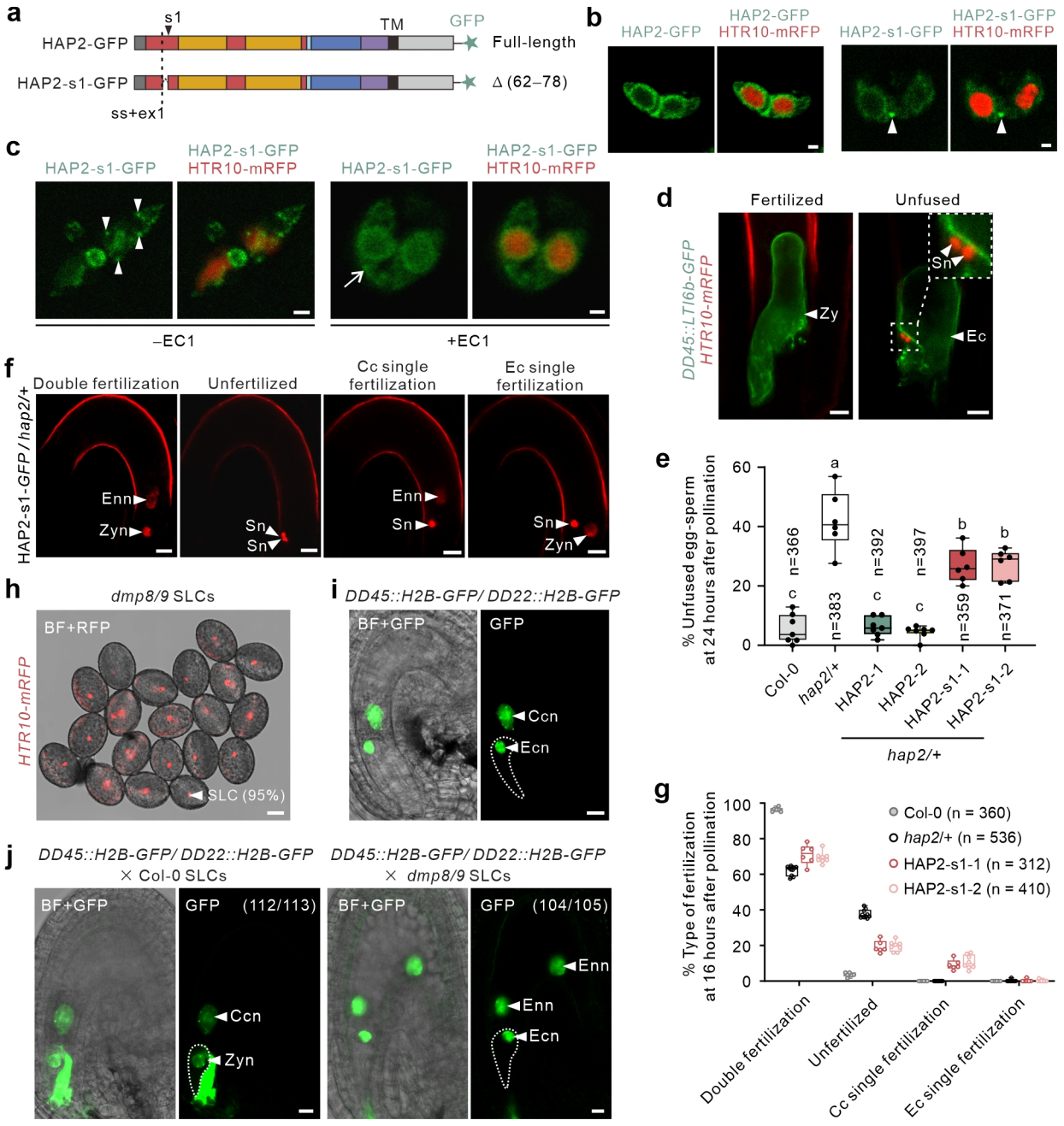



**Fig. 3 ECS-mediated cleavage of HAP2-ECD blocks sperm-egg fusion while maintaining sperm-central cell fusion.**

**a**, Schematic of HAP2-s1-GFP variant lacking the ECS cleavage site s1. **b**, Localization of HAP2-GFP and HAP2-s1-GFP in *HTR10-mRFP* labeled sperm cells. **c**, Following EC1 peptide treatment, HAP2-s1-GFP was recruited from intracellular vesicle-like structures (arrowheads, –EC1) to the sperm plasma membrane (arrow, +EC1). **d**, Elongated Col-0 (wild-type) zygote at 24 hours after pollination with the plasma membrane labeled by GFP-LTI6b (left), and a representative gamete-

765 fusion defect in GFP-LTI6b ovules pollinated with HAP2-s1-GFP sperm cells marked by *HTR10-*
766 *mRFP* (right). **e**, Proportions of unfused egg-sperm pairs at 24 hours after pollination. The data are
767 shown as the mean ± SD. Different letters indicate significant differences ($P < 0.05$, Tukey-Kramer
768 test). **f**, Representative single-fertilization events produced by HAP2-s1-GFP/*hap2/+* pollen
769 containing *HTR10-mRFP* labeled sperm nuclei at 16 hours after pollination. **g**, Statistics of
770 fertilization events at 16 hours after pollination. **h**,**i**, A line containing single sperm-like cells
771 (SLCs) in *NTL11ΔC*-overexpression *HTR10-mRFP / dmp8/9* pollen (**h**) was used to pollinate a
772 line carrying *pDD45::H2B-GFP*-labeled egg cell nuclei and *pDD22::H2B-GFP*-labeled central
773 cell nuclei in Col-0 ovules (**i**). **j**, *dmp8/9* SLCs preferential fertilized the central cell at 24 hours
774 after pollination. BF, bright-field; Cc, central cell; Ccn, central-cell nuclei; Ec, egg cell; Ecn, egg-
775 cell nuclei; Enn, endosperm nucleus; ex1, first exon; Sn, sperm nucleus; ss, signal peptide
776 sequence; TM, transmembrane domain; Zy, zygote; Zyn, zygote nucleus. Scale bars, 1 μm (**b** and
777 **c**), 5 μm (**d**), 10 μm (**f**, **h**–**j**).
778

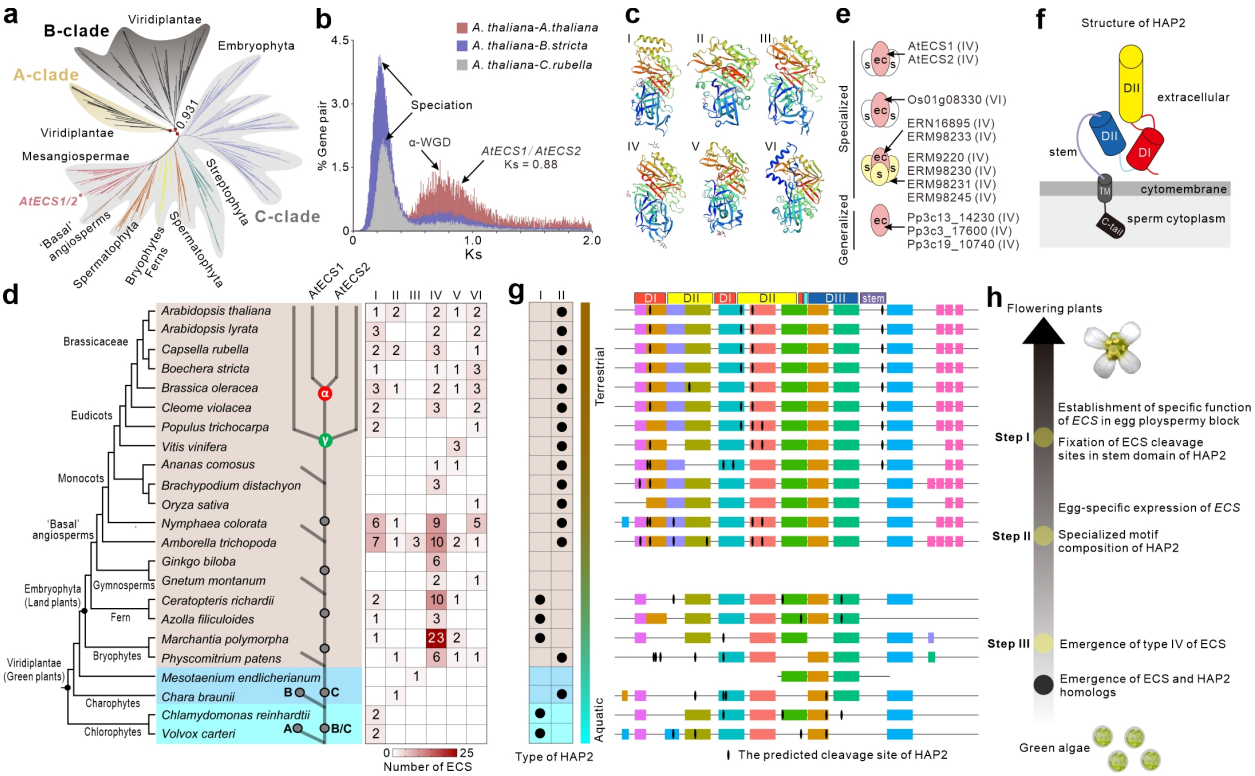



**Fig. 4 Evolution of the ECS-HAP2-mediated block to polyspermy (polygamy) occurred in three steps in green plants.**

**a**, Unrooted phylogenetic tree of the gene family encoding aspartic proteases (APs) in representative taxonomic lineages of green plants (Viridiplantae). The AP family in Viridiplantae could be divided into three major subfamilies (Red dot): AP-A-, AP-B-, and AP-C-clade. AtECS1/2 belong to the AP-C family. **b**, Density distributions of synonymous substitution rate (*Ks*) of all syntenic gene pairs in Brassicaceae. Arrows indicate a putative whole-genome duplication event (α-WGD) that occurred in the most common ancestors of Brassicaceae, and a speciation event that occurred in the Brassicaceae around 39 million years ago[66]. The *Ks* of AtECS1/2 is highlighted by arrows. **c**, Model of predicted 3D-structures of ECSs in green plants. Six types of ECSs were identified and named according to their order of occurrence in the phylogeny tree. Protein sequences from N- to C-terminal region are marked with blue, cyan, green, yellow, orange and red successively. **d**, Representative phylogeny of the evolution of AP genes in green plants inferred from 1232 single copy genes of 23 species surveyed. Major duplications of *ECS* including a core eudicot whole-genome triplication event (γ-WGT) and α-WGD event specific to the Brassicaceae are indicated (left). The evolution of ECSs from Type I to Type VI in (**c**) and the number of genes for each type are shown for the 23 representative species selected. **e**,

Detection of *ECS* transcripts in egg cells of four model land plants. ec, egg cell; s, synergid. **f**, Schematic sketch showing the different domains of HAP2. **g**, Domain structure of HAP2s in 21 selected species (aligned according to **d**). Note that HAP2 homologs could not be detected in gymnosperms. Each species contains either Type I or Type II HAPs (left). Predicted cleavage sites of APs in HAP2s are indicated (right). **h**, Summary of the momentous events that occurred both in ECS and HAP2 emergence and co-evolution of domain structure composition which shaped the extant efficient ECS-HAP2 polyspermy (polygamy) block in dicotyledonous plants. Images of *C. reinhardtii* and *A. thaliana* were used to represent green algae and flowering plants, respectively.

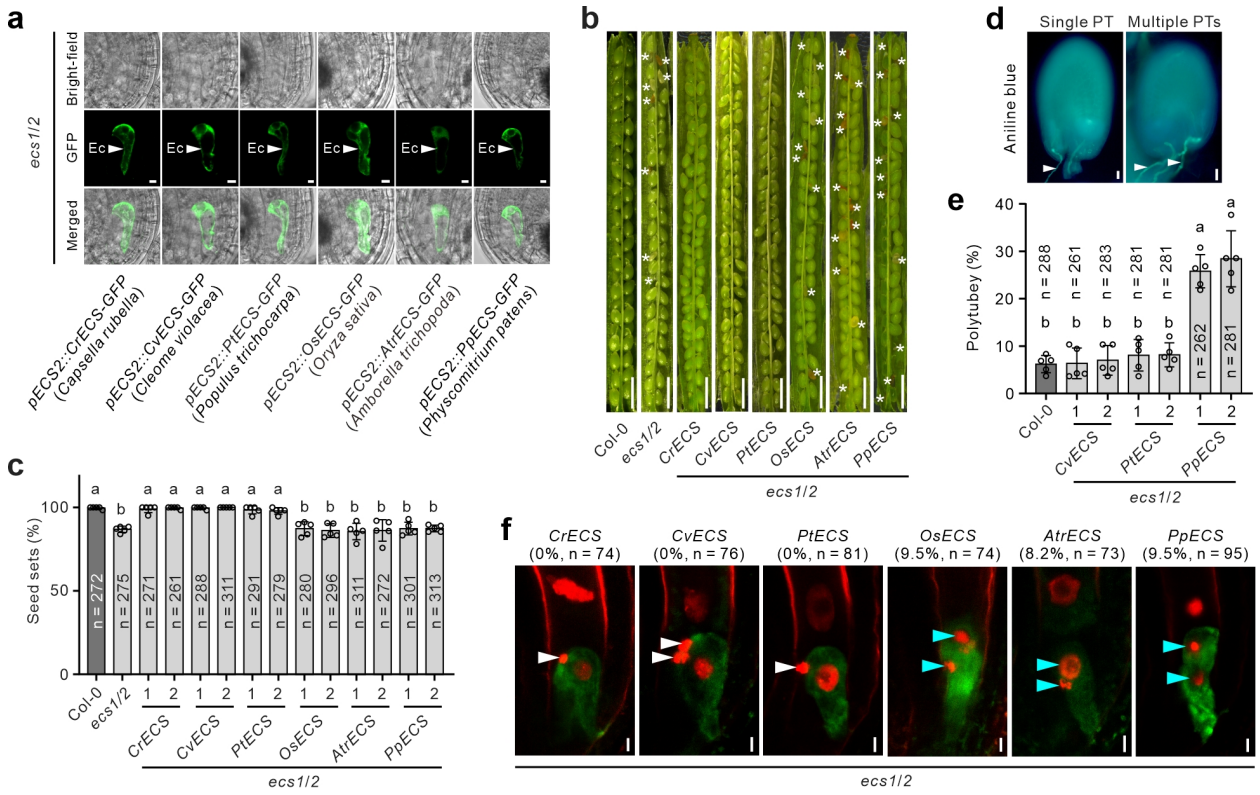



**Fig. 5 Lineage-specific functional specialization of ECS proteins during plant evolution.**

**a**, ECS-GFP from different species expressed in the egg cells (Ec, arrowheads) of *ecs1/2* mutants under the control of *Arabidopsis ECS2* promoter. **b**, ECS-GFPs of Brassicaceae, but not of grasses, *Amborella* or moss, complemented the seed sets of the *ecs1/2* mutants' phenotype. Asterisks indicate abnormal seeds. **c**, Quantification of seed-set complementation shown in (**b**). **d** and **e**, Polytubey phenotype (**d**) and quantification (**e**) in Col-0, *ecs1/2*, and *ecs1/2* lines with expressing ECS-GFPs in egg cells. Arrowheads indicate pollen tubes (PTs). **f**, Frequency of egg polyspermy in the compensatory lines shown in (**a**) after pollination with *tes* pollen. Ovules with multiple sperm entering the embryo sac were analyzed. White arrowheads indicate additional sperm remaining outside the eggs. Cyan arrowheads indicate multiple sperm entering the eggs. Data in (**c**) and (**e**) are shown as the means ± SD. Different letters indicate significant differences ($P < 0.05$, Tukey-Kramer test). Scale bars, 5 μm (**a** and **f**), 1 mm (**b**), 10 μm (**d**).

## Supplementary Files

This is a list of supplementary files associated with this preprint. Click to download.

- Supplementarymaterials.pdf